Multiscale measurements of hurricane waves using buoys and airborne radar

Jacob R. Davis
Applied Physics Laboratory
University of Washington
Seattle WA, USA
davisjr@uw.edu

Jim Thomson
Applied Physics Laboratory
University of Washington
Seattle WA, USA
jthomson@apl.washington.edu

Brian J. Butterworth
CIRES
University of Colorado Boulder, and
Physical Sciences Laboratory
NOAA
Boulder CO, USA
brian.butterworth@noaa.gov

Isabel A. Houghton
Sofar Ocean
San Francisco CA, USA
isabel.houghton@sofarocean.com

Chris Fairall
Physical Sciences Laboratory
NOAA
Boulder CO, USA
chris.fairall@noaa.gov

Elizabeth J. Thompson
Physical Sciences Laboratory
NOAA
Boulder CO, USA
elizabeth.thompson@noaa.gov

Gijs de Boer
CIRES
University of Colorado Boulder, and
Physical Sciences Laboratory
NOAA
Boulder CO, USA
gijs.deboer@noaa.gov

2024 IEEE/OES Thirteenth Current, Waves and Turbulence Measurement (CWTM) | 979-8-3503-9391-0/24/$31.00 ©2024 IEEE | DOI: 10.1109/CWTM61020.2024.10526332

***Abstract*—The processes important to hurricane wave generation cover scales from kilometers to centimeters. Within a storm, waves have complex spatial variations that are sensitive to hurricane size, strength and speed. This makes it challenging to measure the spatial variability of hurricane waves with any single instrument. To obtain both broad spatial coverage and resolve the full range of wave scales, we combine arrays of drifting wave buoys with airborne radar altimetry. The microSWIFT (UW-APL) and Spotter (Sofar) buoys are air-deployed along a given storm track. These buoys resolve the scalar wave frequency spectrum from 0.05 Hz to 0.5 Hz, which is approximately 600 m to 6 m wavelength (in deep water). The Wide Swath Radar Altimeter (WSRA) flies into hurricanes aboard the NOAA Hurricane Hunter P-3 aircraft. The radar altimetry data is processed to produce a 2D directional spectrum from 2.5 km to 80 m wavelength, and the radar backscatter provides an estimate of the mean square slope down to centimeter wavelengths. We introduce a method to use colocated mean square slope observations from each instrument to infer the shape of the spectral tail from 0.5 Hz to almost 3 Hz. The method is able to recover the frequency f^{-5} tail characteristic of the saturation range expected at these frequencies (based on theory and measurements in lower wind speeds). We also explore the differences between WSRA and buoy mean square slopes, which represent the mean square slope of the intermediate wavelength waves (6 m down to 20 cm). Together, the fusion of these wave measurements provides a multiscale view of the hurricane-generated waves. These ocean surface waves are critical as drivers of the air-sea coupling that controls storm evolution and as drivers of coastal impacts by hurricanes.**

***Index Terms*—surface waves, buoys, radar, hurricanes**

Funding provided by the U.S. National Ocean Partnership Program (NOPP) as part of the NOPP Hurricane Coastal Impacts project.

I. Introduction

The ocean surface wave energy spectrum spans wavelengths from kilometers to millimeters. The tail of the spectrum is important for understanding wave-induced stress [1]–[3]. The canonical tail of the scalar wave frequency spectrum is typically described in terms of two distinct regions which have different dynamic balances: the *equilibrium range* and the *saturation range*. The equilibrium range arises due to a balance of wind input, dissipation from breaking, and nonlinear energy fluxes, and is characterized by an f^{-4} tail in frequency [4], [5]. The higher frequency saturation range follows the equilibrium range, as marked by a "transition frequency". Within the saturation range, wind input is balanced by dissipation from breaking, and the spectrum has an f^{-5} tail which extends to the high frequency, short gravity waves [6]–[8].

A. 1-D wave spectra in hurricanes

Observations show hurricane wave spectra are mostly unimodal (e.g., [9], [10]), though there are notable exceptions, particularly on the left side of the storm where the wind-sea and swell are propagating in different directions, resulting in two distinct peaks [11]. In [10], the authors fit a JONSWAP spectral model to buoy data and find the spectral tails steepen

from f^{-4} to f^{-5} with decreasing wave age (defined as the ratio of 10-m wind speed to the phase speed at the spectral peak). The mean tail exponent of all their observations is -4.68. Hwang et al. find substantial scatter in their observed spectral slopes (between -4 and -5), and instead suggest the treatment of the spectral slope exponent as a random variable [12]. The Gaussian fit to their data has a mean of -4.48 and standard deviation of 0.53. Drifting buoy observations from hurricanes suggest that the spectral tail is dominated by the f^{-5} saturation range beyond 30 m s^{-1} [13]. Aside from variation across reported measurements, these observations do not extend beyond 0.5 Hz (waves shorter than 6 m).

B. Mean square slope

The mean square slope (mss) of the ocean surface is a high-order moment of the spectrum which is closely related to the tail. When resolved down to sufficiently small wavelengths, mss is widely interpreted as a measure of roughness [1], [14]–[17]. It has also been suggested that mean square slope is related to form drag, which can contribute substantially to the total stress [18]–[20].

Mean square slope can be calculated from the wavenumber spectrum as

$$\mathrm{mss} = \int_{k_1}^{k_2} k^2 E(k) \mathrm{d}k \tag{1}$$

where $E(k)$ is the ocean wave energy spectrum as a function of wavenumber, k, and k_1 and k_2 define the wavenumber extent over which the spectrum, and thus mss, is resolved. Using the deep water dispersion relationship, $\omega^2 = gk$, where $\omega = 2\pi f$ is angular frequency and g is the acceleration of gravity, mss (1) can be expressed as a function of the frequency spectrum

$$\mathrm{mss} = \frac{(2\pi)^4}{g^2} \int_{f_1}^{f_2} f^4 E(f) \mathrm{d}f \tag{2}$$

where $E(f)$ is the wave energy spectrum as a function of frequency, f. Mean square slope is highly sensitive to the scale of the waves and therefore the magnitude varies across instruments which resolve different wavenumber ranges. It is less sensitive to the lower limit, since long waves contribute little to the mss magnitude [8].

Pioneering work by Cox and Munk [14] used photographs of sun glitter on the ocean surface collected from an airplane to calculate the slope distribution at 12.5 m wind speeds from 2 m s^{-1}to 14 m s^{-1}. Their results show the distribution of wave slopes is nearly Gaussian, and that the variance of the distribution, the mss, increases linearly with wind speed. The optical-nature of their measurements suggest this approaches an estimate of the *total* mean square slope (the mss of the wave spectrum down to the smallest waves in the gravity-capillary and capillary wave regimes). They repeated their experiment in the presence of an oil-slicked surface, which was found to reduce mss by a factor of 2-3. The slick suppresses wavelengths shorter than $\sim$0.3 m [1]. The Cox and Munk mean square slopes have since been corroborated by modern measurement techniques (e.g., lidar, polarimetry, radar, satellite-based radiance) [21]–[24]. These works agree that mean square slope has a linear dependence on wind speed in winds less than 20 m s^{-1}.

C. Radar-derived mean square slope

Radar-based remote sensing has been used to make estimates of the sea surface slope distribution for several decades (e.g., [25]). Radar are useful for characterizing the surface slope of smaller waves (centimeter-scale), particularly since they can be applied in challenging conditions such as hurricanes [26], [27].

Radar backscatter is proportional to the probability density of surface wave slopes from which the mean square slope can be determined using an optical model [28], [29]. The radar-estimated mean square slope depends on the scattering regime (e.g., Bragg scattering or quasi-specular) and the wavelength resolution is limited by the radar wavelength.

Jackson et al. [30] estimated mss using Ku-band radar and reported a linear fit. Their mean square slope estimates are equivalent to (1) integrated from small wavenumbers (large wavelengths) to an upper wavenumber of 63 rad m^{-1} (0.1 m wavelength). Observations from [31] using Ka-band radar (upper wavenumber of 250 rad m^{-1} or 0.02 m wavelength) and [15] using the NASA Scanning Radar Altimeter at Ku-band have instead reported a logarithmic dependence on wind speed below 15 m s^{-1}. The logarithmic relationship is in better agreement with the laboratory observations of [32] than with those of Cox and Munk. Similarly, a power-law dependence was reported by [33] using C-band radar (upper wavenumber of 51 rad m^{-1}, 0.12 m wavelength) later supported by [34].

D. Observations at higher wind speeds

There are few reported estimates of the high frequency spectral tail (frequencies $>$ 0.5 Hz) or of the mean square slope beyond 15 to 20 m s^{-1}. The lack of such estimates in extreme wind speeds has made it challenging to validate the use of spectral wave models, which require an empirical tail at these frequencies, in hurricanes [2], [35].

Global positioning system reflectometry (GPS-R), L-band observations of mean square slope have been made in hurricanes in wind speeds up to 59 m s^{-1} [36]–[38]. The GPS-R mss estimates follow a logarithmic form and represent an upper wavenumber of approximately 11 rad m^{-1} (0.57 m). Buoy-based estimates of mss (upper limit 1 rad m^{-1}, 6.2 m) measured in hurricanes effectively saturate beyond 25 m s^{-1}and can be described using a $\tanh$ relationship up to 54 m s^{-1} [13]. Additional, radar-based high wind characterizations of mean square slope appear to be on the horizon (e.g., KaIA and CYGNSS) [39], [40].

Here we combine hurricane wave observations from buoys and airborne radar to characterize the mean square slope at intermediate wavelengths (6 m to 0.2 m) in high wind speeds. We then introduce a method to use colocated mss observations to infer the slope of the high-frequency spectral tail at these wavelengths (approximately 0.5 Hz to 2.8 Hz).

II. Methods

A. Buoys

Hurricane wave buoy observations are from two types of small, free-drifting wave buoys: the microSWIFT (UW-APL) and Spotter (Sofar). Each uses GPS-derived elevations and velocities to estimate wave elevation. Every hour, the wave elevations are processed into spectra which are telemetered through the Iridium satellite network.

The microSWIFT buoy is an expendable wave buoy sized for deployment through the dropsonde chute of scientific aircraft [41]. The buoy is cylindrical with an 8.9 cm diameter, 51.0 cm length, and a mass of 2.9 kg. Wave elevation time series collected at a rate of 4 Hz are transformed to spectra using 256 s windows each with 75% overlap. The spectra are then frequency-merged and output in 42 bins spanning frequencies of 0.05 Hz to 0.5 Hz.

The Sofar Spotter is a sphere-like buoy which is 42 cm in diameter has a mass of 7.5 kg, including ballast [42]. When air-deployed, the Spotters are specially rigged for deployment through an open door [43]. Raw data collected at 2.5 Hz sampling rate and processed into 256-sample FFTs. The final spectra span 0.0293 Hz to 0.5 Hz in 38 bins. A constant frequency resolution of df = 2.5/256 Hz is used up to 0.33 Hz, beyond which the resolution is coarsened to 3 df for bandwidth efficiency when transmitting over the Iridium network.

Data from the full-sized v3 SWIFT buoys collected during ATOMIC were used to evaluate the proposed spectral tail extrapolation method in moderate conditions [44]. The v3 SWIFTs have a 0.35 m diameter hull and a 1.25 m draft [45]. Wave spectra are reported at 42 frequency bins (0.01 Hz to 0.05 Hz) from 8-minute time series of wave elevation. Multiple spectra within a comparison period are averaged, where applicable.

B. Wide Swath Radar Altimeter

The Wide Swath Radar Altimeter (WSRA) is a 16.15 GHz (Ku-band) radar which flies into hurricanes aboard one of the Hurricane Hunter P-3s [26], [46], [47]. It uses altimetry to estimate the 2-D directional wavenumber spectrum from 2.5 km wavelength down to 80 m. The spectra represent an approximately 14 km^2 area collected over 50s and are corrected for Doppler shift as well as a skewing effect which occurs as the radar scans perpendicular to wave crests.

The WSRA also uses backscatter to estimate mean square slope based on the geometric optics model which relates the normalized radar cross section per unit area (σ_0) to mean square slope [28]:

$$\sigma_0 = \frac{|R(0°)|^2}{\text{mss}} \sec^4\theta \exp\left(\frac{-\tan^2\theta}{\text{mss}}\right) \tag{3}$$

where $|R(0°)|^2$ is the Fresnel reflection coefficient at normal incidence, θ is the off-nadir angle, and mss is the mean square slope. Under this assumption, when the logarithm of σ_0 is plotted against $\tan^2\theta$, mean square slope is inversely proportional to the slope. In practice, this is done using a fit through the data [47].

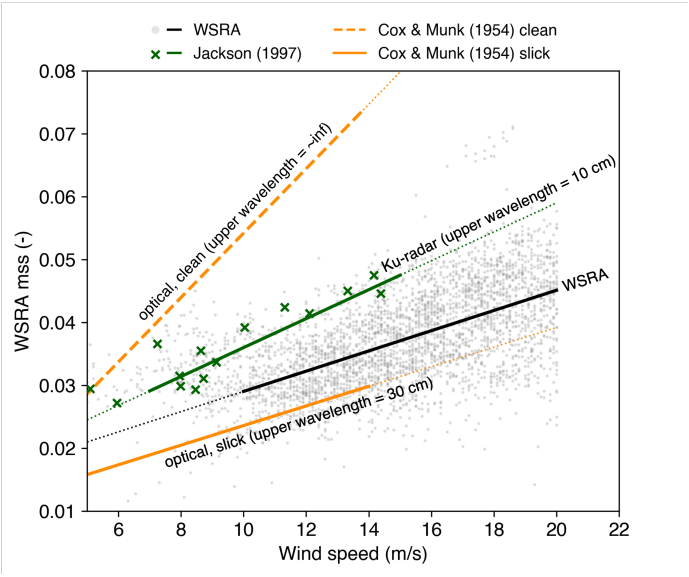

Fig. 1. WSRA mean square slopes compared to those from Cox and Munk (1954) and Jackson et al. (1992) [14], [30]. The black line represents a linear fit to the WSRA data (grey points) from 10 to 20 m s^{-1}. The WSRA mss falls between that of the Jackson et al. (1992) Ku-radar measurements, rigorously determined to have an upper wavelength of 10 cm, and the "slick" sea surface measurements of Cox and Munk (1954) which extend to 30 cm. Linear fits to the mss data are given by: $\text{mss} = 0.003 + 0.00512U_{12.5}$ for $U_{12.5} \in [2, 14]$ m s^{-1}(Cox and Munk, clean), $0.008 + 0.00156U_{12.5}$ (Cox and Munk, slick), $0.013 + 0.0023U_{10}$ for $U_{10} \in [7, 15]$ m s^{-1}(Jackson), and $0.013 + 0.0016U_{10}$ for $U_{10} \in [10, 20]$ m s^{-1}(WSRA).

For the WSRA, this calculation is restricted to off-nadir angles from 0 deg to 14 deg (where 0 deg is pointing directly down at nadir) such that the scattering remains within the quasi-specular regime. When determined using this model, the mean square slope estimate is not sensitive to the calibration of the radar and is likely less sensitive to rain attenuation since all the returns are attenuated by a similar amount. A minor correction is applied to account for the slightly increased path length further off nadir.

In this scattering regime, the estimated mean square slope represents (1) integrated from approximately the width of the swath (100's of meters) down to several times the radar wavelength, λ_r (diffraction limit) [30]. For WSRA, the radar wavelength is λ_r = 1.85 cm. The exact upper wavelength is often not well known and estimates in the literature range from 2 to 10 times λ_r [30], [31], [33]. By comparing to prior estimates of mean square slope with known extents, we determine that the upper wavelength resolved by the WSRA is on the order of 0.2 m (20 cm) (Figure 1). This corresponds to 10.8 λ_r. The upper limit is sensitive to range of off-nadir angle (which is constant) and possibly wind [33], [48].

C. Colocated observations

Colocated buoy and WSRA observations are from three datasets. Buoy observations in hurricanes are from targeted air deployments into Hurricane Ian (2022) and Hurricane Idalia (2023) as part of the NOPP Hurricane Coastal Impacts project (NHCI). The microSWIFT and Spotter buoys intersected with

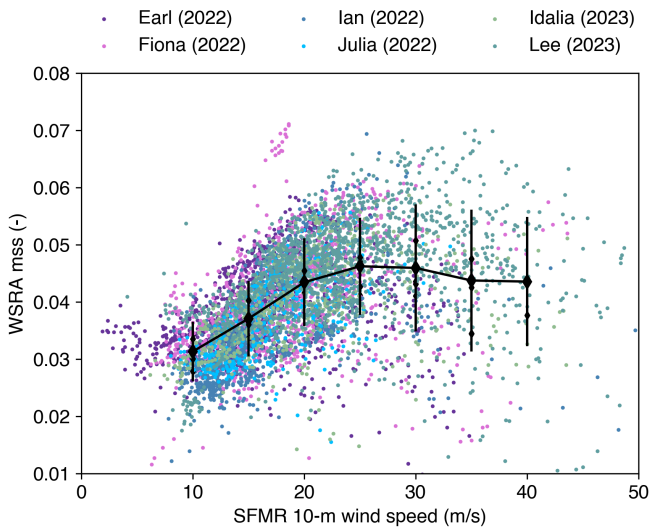

Fig. 2. WSRA mean square slopes versus SFMR 10-m wind speed, colored by hurricane. Black diamonds indicate bin-averages from the combined data, and the error bars represent one standard deviation in each bin.

the flight path of the NOAA Hurricane Hunter P-3 carrying the WSRA (H1 and and I1 planes in Ian and Idalia, respectively). The colocated observations are within a 100 km radius and 90 minutes of one another. Additional data from the Atlantic Tradewind Ocean-Atmosphere Mesoscale Interaction Campaign (ATOMIC) (2020) are included for evaluation of the tail extrapolation method at lower wind speeds. The ATOMIC field campaign took place in the tropical North Atlantic east of Barbados January through February 2021 [44], [49]. Several flight tracks from the P-3/WSRA are directly overhead of the SWIFT drifters.

III. Mean Square Slope Versus Wind Speed

A. WSRA mean square slope

WSRA data from hurricanes Earl (2022), Fiona (2022), Ian (2022), Julia (2022), Idalia (2023), and Lee (2023) are combined with 10-m wind speed estimates from the stepped frequency microwave radiometer (SFMR) which flies concurrently aboard the NOAA P-3s [50]. The WSRA data are filtered to remain within limits for aircraft roll ($\pm 2.5°$), altitude (1000-4000 m), groundspeed (80-250 m s^{-1}), and rainfall rate (< 50 mm hr^{-1}). Rainfall rate estimates from both the SFMR and WSRA are used for filtering purposes. SFMR wind speed observations flagged as invalid were excluded.

WSRA mean square slopes measured in all six hurricanes saturate at high wind speeds and, in many cases, reduce at the highest wind speeds (Figure 2). Bin-averages, which include data from all hurricanes, reach a maximum around 25 m s^{-1}, beyond which they reduce slightly and then level-off around 35 m s^{-1}. The WSRA mss wind speed dependence is similar to that of the L-band GPS-R mss summarized in [38], though the WSRA mss is higher due to its higher upper wavenumber (31.4 rad m^{-1} compared to 11 rad m^{-1}). Deviation from the linear dependence on wind speed (above 20 m s^{-1}) in the WSRA mss hurricane datasets presented here and from GPS-R are qualitatively similar to those measured by drifting buoys [13].

B. Mean square slope at intermediate wavelengths

WSRA mss represents waves with lengths from several hundred meters down to 0.2 m (20 cm). While the exact lower limit is not well-defined, the extent overlaps with the wavelengths measured by buoys, 600 m to 6 m. Assuming the WSRA longer wavelength limit is comparable to that of the buoy, and that these waves have little contribution to the overall mss, the difference of the WSRA mss and buoy mss should approximate the mss of waves between 6 m and 0.2 m. The difference between the mss measurements also saturates with 10-m wind speed (Figure 3). The results agree with a set of similar, yet lower wind speed, observations from [31] which represent the difference of a Ka-band radar mss (0.02 m lower wavelength) and a laser altimeter mss (2 m lower wave length) and thus waves from 2 m to 0.02 m. The authors report a logarithmic fit to their data.

IV. Spectral Tail Extrapolation

Buoys measure the energy spectrum in frequency from 0.05 Hz to 0.5 Hz. Since mean square slope in (2) is proportional to the area beneath an Ef^4 spectrum, colocated observations of WSRA mss and buoy mss, which overlap in frequency extent, can be used to infer information about the spectral tail beyond 0.5 Hz. In particular, colocated observations of the difference between WSRA mss and buoy mss (Figure 3) can be used to constrain the spectral slope from 0.5 Hz to 2.8 Hz (from 6 m to 0.2 m in deep water).

The difference of the WSRA and buoy mean square slopes is defined as

$$\mathrm{mss}_\delta = \mathrm{mss}_{\mathrm{WSRA}} - \mathrm{mss}_{\mathrm{buoy}} \tag{4}$$

where $\mathrm{mss}_{\mathrm{buoy}}$ is the mean square slope from the integrated buoy spectrum, which cover frequencies from ~ 0.05 Hz to 0.5 Hz, and $\mathrm{mss}_{\mathrm{WSRA}}$ is the quasi-specular WSRA mean square slope estimate which is assumed to cover $\sim$ 0.05 Hz to 2.8 Hz.

We seek to extend the buoy spectrum, $E_{\mathrm{buoy}}(f)$, with a spectral tail of the form $E_\delta(f) = cf^n$ which starts at the end of the buoy spectrum, $f_1 = 0.5$ Hz, and extends to the frequency of the smallest wavelength resolved by the WSRA mss, $f_2 = 2.8$ Hz. Here c is a constant and n is the unknown slope exponent. When f^4-compensated, $E_\delta(f)f^4$ has the form cf^a where $a = n + 4$ (Figure 4). The integral of cf^a should be equal to the area determined by the mean square slope in (2),

$$\int_{f_1}^{f_2} cf^a df = \frac{c}{a+1}\left(f_2^{a+1} - f_1^{a+1}\right) = \frac{g^2}{(2\pi)^4}\mathrm{mss}_\delta \tag{5}$$

Since the spectrum must be continuous at f_1, then

$$E(f_1)f_1^4 = cf_1^a \tag{6}$$

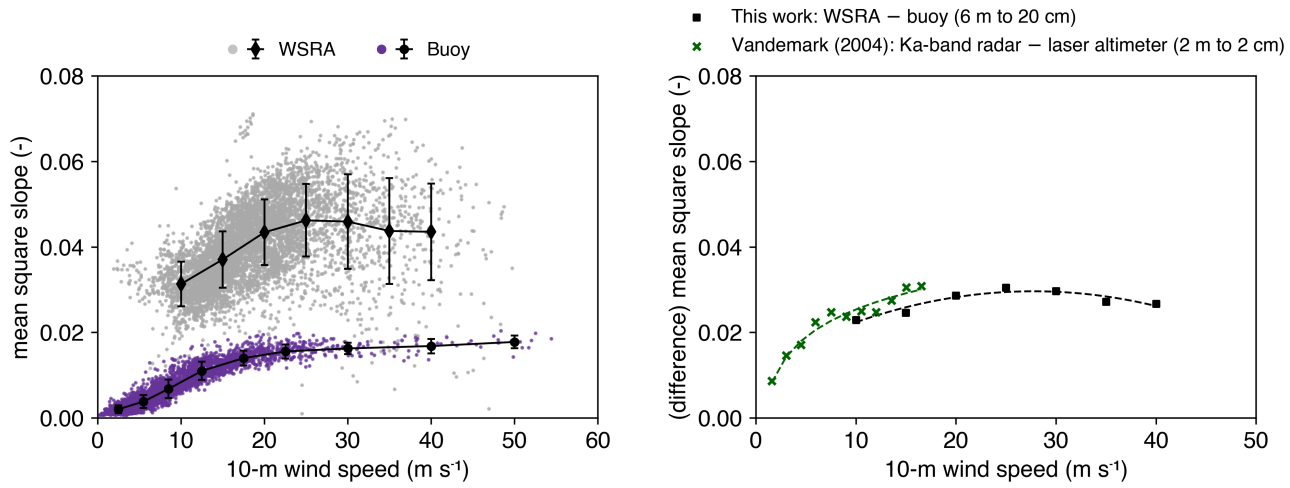

Fig. 3. WSRA mss and buoy mss (left) and their difference (right), which represents waves from 6 m to 20 cm. The difference is calculated from the bin averaged WSRA mss and buoy mss (diamonds and circles on the left plot). Data from Vandemark (2004) are shown for comparison (their Figure 10, "coastal" observations), including the logarithmic fit $0.004 + 0.0093\ln(U_{10})$ for $U_{10} \in [1.5, 16.5]$ m s^{-1} [31]. Lower wind speed WSRA mss observations are required to fit a comparable logarithmic function to the difference of WSRA mss and buoy mss, however the SFMR does not produce reliable U_{10} estimates at low wind speeds [50]. A second-order polynomial fit is shown: $-2.3 \cdot 10^{-5}U_{10}^2 + 0.00128U_{10} + 0.012$. for $U_{10} \in [10, 40]$ m s^{-1}.

such that

$$c = E(f_1)f_1^{(4-a)} \tag{7}$$

Inserting (7) into (5) results in an equation with one unknown, the exponent a, which can be determined by root-finding:

$$\frac{E(f_1)}{a+1}f_1^{(4-a)}\left(f_2^{a+1} - f_1^{a+1}\right) - \frac{g^2}{(2\pi)^4}\mathrm{mss}_\delta = 0 \tag{8}$$

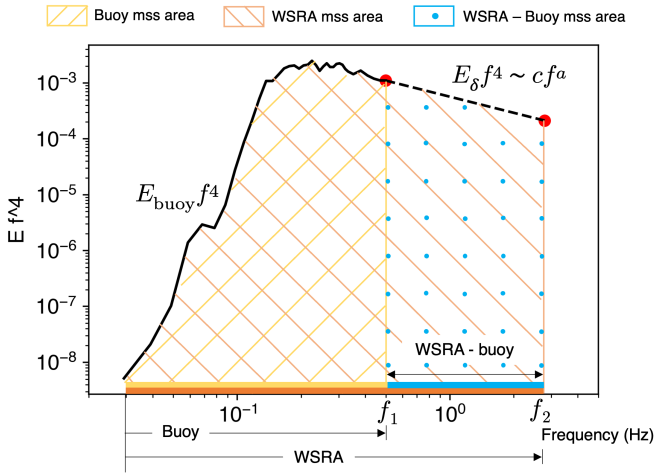

Fig. 4. Extrapolation of the f^4-compensated buoy spectrum, $E_{\mathrm{buoy}}(f)f^4$, with a compensated tail $E_\delta(f)f^4$ of the form cf^a. When compensated, the area beneath the spectrum is proportional to mean square slope (2). The colored bars and shading represent the frequency and mss extent of the buoy (yellow, hatched), WSRA (orange, hatched), and their difference (blue, stippled).

Once a is found, the form of the regular energy spectrum over this frequency extent is then

$$E_\delta(f) = cf^n \tag{9}$$

where $n = a - 4$.

This method was applied to 21 sets of colocated WSRA and buoy observations. Since the WSRA reports mss every minute, all mss observations within a buoy reporting window are used to obtain $\mathrm{mss}_{\mathrm{WSRA}}$. The inferred tail slopes range from n = −4.1 to n = −5.8, with a mean of n = −4.8 and a standard deviation of 0.41. Wind speeds vary from 10.5 m s^{-1}to 25.6 m s^{-1}and buoy-measured significant wave heights span 1.9 m to 6.9 m.

Three examples of the tail extrapolation method, using cases from the ATOMIC campaign (2020), Hurricane Idalia (2023), and Hurricane Ian (2022), are shown in Figure 5. The ATOMIC case (Figure 5A) is in moderate conditions with a mean wind speed of 10.9 m s^{-1}and a buoy-measured significant wave height of 1.93 m. The largest separation distance is 22.14 km, and half of the WSRA flight track is directly over the SWIFT. The 1-D WSRA frequency spectrum, derived from the 2D wavenumber spectrum using the Jacobian to convert wavenumber space to frequency-direction space (e.g., [51]), is shown for comparison. The WSRA spectrum is only resolved from 0.025 Hz to 0.14 Hz (2500 m to 80 m), but has similar energy levels and captures the main peak. The significant wave height reported by the WSRA is 1.79 m, slightly less than that of the buoy.

The Ian and Idalia cases (Figure 5B-C) are characterized by higher wind speeds (22.7 m s^{-1}and 21.9 m s^{-1}, respectively) and more energetic sea states (buoy significant wave heights of 5.0 m and 6.3 m). There is good agreement in the shape and

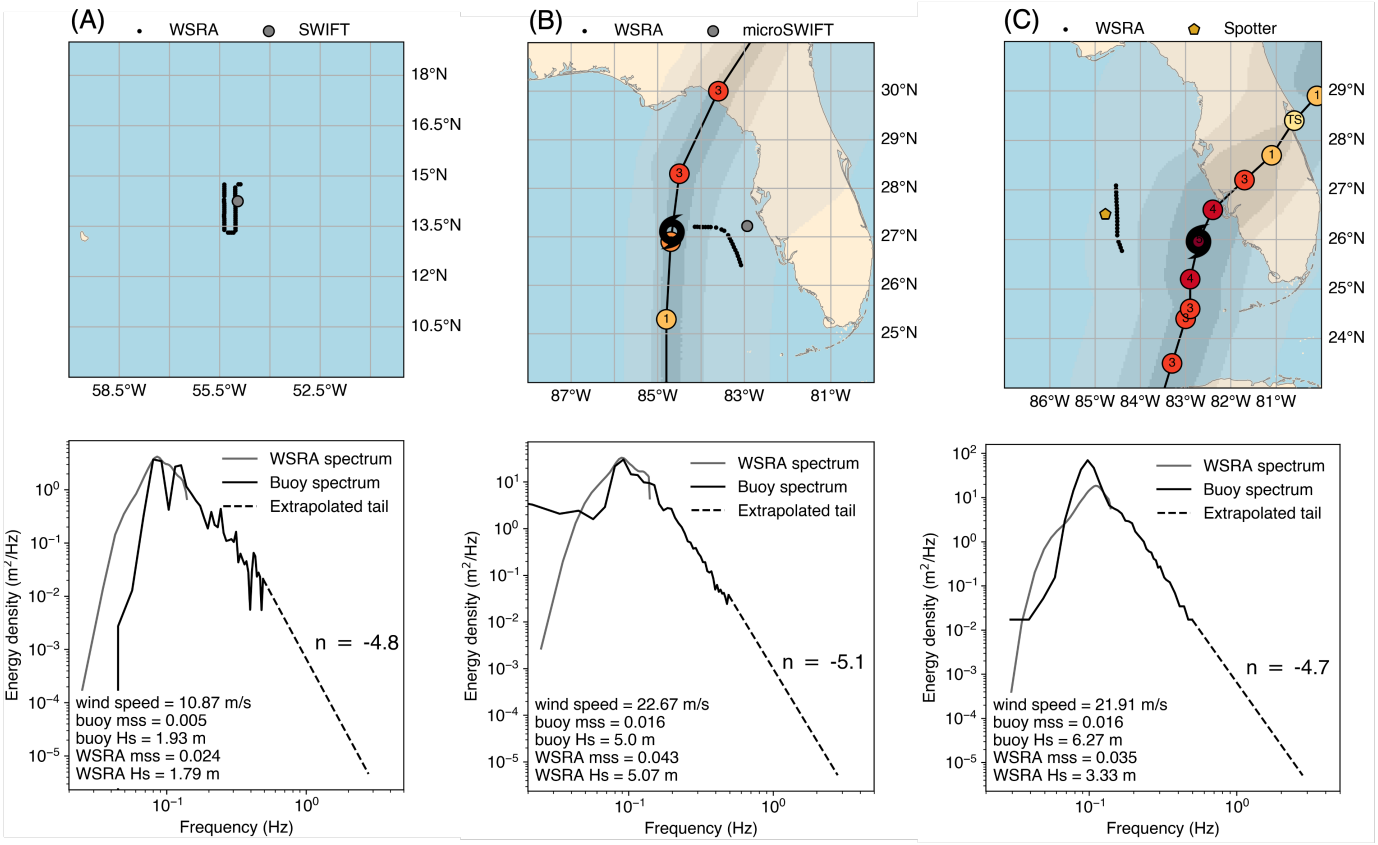

Fig. 5. Slope extrapolation example cases from ATOMIC (A), Hurricane Idalia (B), and Hurricane Ian (C). For each case, the top panels show the WSRA and buoy locations and the bottom panels show the spectra and extrapolated tails. The dashed line represents the $E_\delta(f)$ tail and n corresponds to the inferred spectral slope exponent in cf^n.

energy levels of the 1D spectra and significant wave height between WSRA (5.1 m) and the microSWIFT buoy (5.0 m) in the Ian case. The mean distance between the observations is 68.64 km. In the Idalia case, however, the WSRA spectrum has lower overall energy levels and a higher peak frequency than the Spotter buoy. The WSRA-reported significant wave height (3.3 m) is nearly half that of the buoy (6.3 m). The mean separation distance, 51.49 km, is lower than in Ian.

V. Discussion and Conclusions

The saturation of WSRA mean square slope (wavelengths $>$ 0.2 m) with wind speed in hurricanes is consistent with the behavior of buoys ($>$ 6 m) (Figures 2 and 3) [13]. The wind speed at which the WSRA mean square slopes saturate is higher than that of the buoys (approximately 25-30 m s^{-1}compared to 20 m s^{-1}) which may be due to the evolution of the intermediate wavelengths (6 m to 0.2 m) resolved by the WSRA but not the buoy.

The mss of these intermediate wavelengths is represented by the difference of the WSRA mss and buoy mss which also ceases to increase beyond 25 m s^{-1}(Figure 3). The data are in general agreement with a set of similar measurements from [31] which are described by a logarithmic wind speed dependence below 18 m s^{-1}. This suggests it is not just the mss of the larger waves which saturate at the extreme wind speeds found in hurricanes. The difference between WSRA mss and buoy mss is likely more representative of roughness (typically associated with shorter waves) [18]. Following the interpretation of mean square slope as a measure of surface roughness, the saturation and roll-off captured in both the WSRA mss and difference between the WSRA mss and buoy mss is consistent with the qualitatively similar behavior of the sea surface roughness length first observed by [52]. The WSRA mss, however, contains slope information that may be relevant to both form and viscous components of the drag.

The mean square slope of the intermediate waves can be used to extrapolate the tail of the buoy spectrum by inferring a constant spectral slope over the frequencies 0.5 Hz to 2.8 Hz. When the equilibrium-to-saturation transition frequency is higher than 0.5 Hz, the constant spectral shape assumption does not hold. However the transition frequency decreases with increasing wind speed [23], [53] and is consistently lower than 0.5 Hz beyond 12 m s^{-1}in the data of [53].

The mean spectral slope ($n = -4.8$) from 21 colocated WSRA-buoy pairs (within 100 km and 90 minutes), as well as the examples from ATOMIC ($n = -4.8$), Idalia ($n = -5.1$), and Ian ($n = -4.7$) are all close to the canonical f^{-5} tail anticipated at these frequencies. In the ATOMIC

case, there is generally good agreement between the energy levels of the WSRA and buoy 1D WSRA frequency spectra as well as between the reported significant wave heights (Figure 5A). However the ATOMIC wave conditions were sometimes characterized by two separate wave systems (swell from the north and wind sea from the east), and it appears the higher frequency peak was not captured by WSRA. Good agreement is also observed in the Idalia case, though the wind speed and significant wave height are much higher (22.7 m $s^{-1}$and 5 m, respectively) (Figure 5B).

There is substantial disagreement between WSRA and buoys in the Ian example (Figure 5C). The WSRA misses the peak and has far lower energy levels, reporting a significant wave height of only 3.3 m relative to the 6.3 m reported by the buoy. The latter is much more typical of hurricane waves, and it is unlikely the observations are close enough to the hurricane eye for a gradient this large to be realistic [10]. Further, the WSRA observations are also closer to the hurricane than the buoy. Still, the WSRA mss (0.035) is comparable to the other two cases and is close to being within a standard deviation of the observations shown in Figure 2. The WSRA mss estimate from the backscatter is upstream of the spectral estimate in the WSRA processing pipeline and does not require correction for the skewing effect caused by the waves during altimetry [47]. This suggests the WSRA mss, and thus the spectral tail extrapolation method, may still yield reasonable values despite poor wave height estimates.

Despite good agreement with the canonical result, several sources of uncertainty remain. The exact lower and upper wavenumber limits of the WRSA mss, and whether they may be evolving with wind speed (e.g., [33]), are not well-known. Uncertainty may be narrowed through more careful examination of raw backscatter data to determine the diffraction limit (upper wavenumber), as was done in [30]. Errors are introduced by separation in space and time, especially in hurricane sea states, and since the mss response time can be well under an hour [54]. This motivates more carefully colocated wave buoys and airborne WSRA in future hurricanes.

Narrowing errors, this method can be used to understand the evolution of the spectral tail in high winds, and its dependence on factors such as storm size, speed, and strength. A better-parameterized tail will enable more accurate parameterization of stress in models which require a prescribed tail [2], [3].

A. Data Availibility

Wide Swath Radar Altimeter data can be accessed from https://www.prosensing.com/wsra-level-4-data and the accompanying met data can be downloaded from https://seb.noaa.gov/pub/acdata/2023/MET/. Spotter and microSWIFT data from Hurricane Ian are available at https://orcid.org/0000-0001-8623-2141. SWIFT data from ATOMIC are at https://doi.org/10.5194/essd-13-3281-2021 [49] and WSRA data are at https://doi.org/10.5194/essd-13-1759-2021 [44]. A master archive of microSWIFT data, which contains data from additional hurricanes, is at https://datadryad.org/stash/dataset/doi:10.5061/dryad.jdfn2z3j1.

ACKNOWLEDGMENT

This work was funded by the U.S. National Ocean Partnership Program (NOPP) as part of the NOPP Coastal Hurricane Impacts project. Air-support was provided by the Navy VXS-1 Scientific Deployment Squadron via the Naval Research Laboratory.

The authors thank APL-UW engineers Alex de Klerk, Phil Bush, Emily Iseley, and Joe Talbert for preparation and maintenance of SWIFT and microSWIFT buoys in the ATOMIC and NOPP Hurricane Coastal Impacts projects. Spotter data was provided by Sofar Ocean.

This material is based upon work supported by the National Science Foundation Graduate Research Fellowship Program under Grant No. DGE-2140004. Any opinions, findings, and conclusions or recommendations expressed in this material are those of the author(s) and do not necessarily reflect the views of the National Science Foundation.

REFERENCES

[1] P. A. Hwang, "Wave number spectrum and mean square slope of intermediate-scale ocean surface waves," *Journal of Geophysical Research: Oceans*, vol. 110, 2005.

[2] B. G. Reichl, T. Hara, and I. Ginis, "Sea state dependence of the wind stress over the ocean under hurricane winds," *Journal of Geophysical Research: Oceans*, vol. 119, no. 1, pp. 30–51, 2014.

[3] X. Chen, T. Hara, and I. Ginis, "Impact of Shoaling Ocean Surface Waves on Wind Stress and Drag Coefficient in Coastal Waters: 1. Uniform Wind," *Journal of Geophysical Research: Oceans*, 2020.

[4] Y. Toba, "Local balance in the air-sea boundary processes," *Journal of the Oceanographical Society of Japan*, vol. 29, pp. 209–220, 1973.

[5] O. M. Phillips, "Spectral and statistical properties of the equilibrium range in wind-generated gravity waves," *Journal of Fluid Mechanics*, vol. 156, p. 505, Jul. 1985.

[6] G. Z. Forristall, "Measurements of a saturated range in ocean wave spectra," *Journal of Geophysical Research*, vol. 86, no. C9, p. 8075, 1981.

[7] M. L. Banner, "Equilibrium spectra of wind waves," *Journal of Physical Oceanography*, vol. 20, pp. 966–984, 1990.

[8] L. Lenain and W. K. Melville, "Measurements of the Directional Spectrum across the Equilibrium Saturation Ranges of Wind-Generated Surface Waves," *Journal of Physical Oceanography*, vol. 47, no. 8, pp. 2123–2138, Aug. 2017.

[9] I. R. Young, "Directional spectra of hurricane wind waves," *Journal of Geophysical Research: Oceans*, vol. 111, 2006.

[10] A. Tamizi and I. R. Young, "The Spatial Distribution of Ocean Waves in Tropical Cyclones," *Journal of Physical Oceanography*, vol. 50, no. 8, pp. 2123–2139, 2020.

[11] K. Hu and Q. Chen, "Directional spectra of hurricane-generated waves in the Gulf of Mexico," *Geophysical Research Letters*, vol. 38, no. 19, Oct. 2011.

[12] P. A. Hwang, Y. Fan, F. J. Ocampo-Torres, and H. García-Nava, "Ocean Surface Wave Spectra inside Tropical Cyclones," *Journal of Physical Oceanography*, vol. 47, no. 10, pp. 2393–2417, 2017.

[13] J. R. Davis, J. Thomson, I. A. Houghton, J. D. Doyle, W. A. Komaromi, C. W. Fairall, E. J. Thompson, and J. R. Moskaitis, "Saturation of Ocean Surface Wave Slopes Observed During Hurricanes," *Geophysical Research Letters*, vol. 50, no. 16, 2023.

[14] C. Cox and W. Munk, "Measurement of the Roughness of the Sea Surface from Photographs of the Sun's Glitter," *Journal of the Optical Society of America*, vol. 44, no. 11, p. 838, Nov. 1954.

[15] E. J. Walsh, D. C. Vandemark, C. A. Friehe, S. P. Burns, D. Khelif, R. N. Swift, and J. F. Scott, "Measuring sea surface mean square slope with a 36-GHz scanning radar altimeter," *Journal of Geophysical Research: Oceans*, vol. 103, no. C6, pp. 12 587–12 601, Jun. 1998.

[16] O. Boisot, S. Pioch, C. Fatras, G. Caulliez, A. Bringer, P. Borderies, J. Lalaurie, and C. Guérin, "Ka-band backscattering from water surface at small incidence: A wind-wave tank study," *Journal of Geophysical Research: Oceans*, vol. 120, no. 5, pp. 3261–3285, May 2015.

[17] X. Li, V. Karaev, M. Panfilova, B. Liu, Z. Wang, Y. Xu, J. Liu, and Y. He, "Measurements of total sea surface mean square slope field based on SWIM data," *IEEE Transactions on Geoscience and Remote Sensing*, 2022.

[18] M. A. Donelan, M. Curcic, S. S. Chen, and A. K. Magnusson, "Modeling waves and wind stress," *Journal of Geophysical Research: Oceans*, vol. 117, Nov. 2012.

[19] M. A. Donelan, "On the Decrease of the Oceanic Drag Coefficient in High Winds," *Journal of Geophysical Research: Oceans*, 2018.

[20] P. P. Sullivan, M. L. Banner, R. P. Morison, and W. L. Peirson, "Turbulent Flow over Steep Steady and Unsteady Waves under Strong Wind Forcing," *Journal of Physical Oceanography*, vol. 48, no. 1, pp. 3–27, Jan. 2018.

[21] F. M. Bréon and N. Henriot, "Spaceborne observations of ocean glint reflectance and modeling of wave slope distributions," *Journal of Geophysical Research*, vol. 111, no. C6, p. C06005, 2006.

[22] C. J. Zappa, M. L. Banner, H. Schultz, A. Corrada-Emmanuel, L. B. Wolff, and J. Yalcin, "Retrieval of short ocean wave slope using polarimetric imaging," *Measurement Science and Technology*, vol. 19, no. 5, May 2008.

[23] L. Lenain, N. M. Statom, and W. K. Melville, "Airborne Measurements of Surface Wind and Slope Statistics over the Ocean," *Journal of Physical Oceanography*, vol. 49, no. 11, pp. 2799–2814, Nov. 2019.

[24] C.-A. Guérin, V. Capelle, and J.-M. Hartmann, "Revisiting the Cox and Munk wave-slope statistics using IASI observations of the sea surface," *Remote Sensing of the Environment*, Oct. 2022.

[25] F. J. Wentz, "A Two-Scale Scattering Model With Application to the JONSWAP '75 Aircraft Microwave Scatterometer Experiment," NASA Contractor Report, 1977.

[26] E. J. Walsh, I. PopStefanija, S. Y. Matrosov, J. Zhang, E. Uhlhorn, and B. Klotz, "Airborne Rain-Rate Measurement with a Wide-Swath Radar Altimeter," *Journal of Atmospheric and Oceanic Technology*, vol. 31, no. 4, pp. 860–875, Apr. 2014.

[27] P. A. Hwang and Y. Fan, "Low-Frequency Mean Square Slopes and Dominant Wave Spectral Properties: Toward Tropical Cyclone Remote Sensing," *IEEE Transactions on Geoscience and Remote Sensing*, no. 12, 2018.

[28] D. Barrick, "Relationship between slope probability density function and the physical optics integral in rough surface scattering," *Proceedings of the IEEE*, vol. 56, no. 10, pp. 1728–1729, 1968.

[29] Y. Liu, M.-Y. Su, X.-H. Yan, and W. T. Liu, "The Mean-Square Slope of Ocean Surface Waves and Its Effects on Radar Backscatter," *Journal of Atmospheric and Oceanic Technology*, vol. 17, no. 8, pp. 1092–1105, Aug. 2000.

[30] F. C. Jackson, W. T. Walton, D. E. Hines, B. A. Walter, and C. Y. Peng, "Sea surface mean square slope from K_u -band backscatter data," *Journal of Geophysical Research: Oceans*, vol. 97, pp. 11 411–11 427, Jul. 1992.

[31] D. Vandemark, B. Chapron, J. Sun, G. H. Crescenti, and H. C. Graber, "Ocean Wave Slope Observations Using Radar Backscatter and Laser Altimeters," *Journal of Physical Oceanography*, vol. 34, no. 12, pp. 2825–2842, Dec. 2004.

[32] J. Wu, "Mean square slopes of the wind-disturbed water surface, their magnitude, directionality, and composition," *Radio Science*, vol. 25, no. 1, pp. 37–48, 1990.

[33] D. Hauser, G. Caudal, S. Guimbard, and A. A. Mouche, "A study of the slope probability density function of the ocean waves from radar observations," *Journal of Geophysical Research: Oceans*, vol. 113, no. C2, p. 2007JC004264, Feb. 2008.

[34] P. Chen, G. Zheng, D. Hauser, and F. Xu, "Quasi-Gaussian probability density function of sea wave slopes from near nadir Ku-band radar observations," *Remote Sensing of Environment*, vol. 217, pp. 86–100, Nov. 2018.

[35] X. Chen, I. Ginis, and T. Hara, "Impact of Shoaling Ocean Surface Waves on Wind Stress and Drag Coefficient in Coastal Waters: 2. Tropical Cyclones," *Journal of Geophysical Research: Oceans*, 2020.

[36] S. J. Katzberg, J. Dunion, and G. G. Ganoe, "The use of reflected GPS signals to retrieve ocean surface wind speeds in tropical cyclones," *Radio Science*, vol. 48, no. 4, pp. 371–387, Jul. 2013.

[37] S. Gleason, V. U. Zavorotny, D. M. Akos, S. Hrbek, I. PopStefanija, E. J. Walsh, D. Masters, and M. S. Grant, "Study of Surface Wind and Mean Square Slope Correlation in Hurricane Ike With Multiple Sensors," *IEEE Journal of Selected Topics in Applied Earth Observations and Remote Sensing*, vol. 11, no. 6, pp. 1975–1988, Jun. 2018.

[38] P. A. Hwang, T. L. Ainsworth, and J. D. Ouellette, "Microwave Specular Measurements and Ocean Surface Wave Properties," *Sensors*, vol. 21, no. 4, p. 1486, Feb. 2021.

[39] J. Sapp, Z. Jelenak, P. Chang, J. R. Carswell, B. Pollard, and A. Theg, "Near-Real-Time Significant Wave Heights in Hurricanes from a New Airborne KA-Band Interferometric Altimeter," in *2021 IEEE International Geoscience and Remote Sensing Symposium IGARSS*. Brussels, Belgium: IEEE, Jul. 2021, pp. 7426–7429.

[40] H. Carreno-Luengo, J. A. Crespo, R. Akbar, A. Bringer, A. Warnock, M. Morris, and C. Ruf, "The CYGNSS Mission: On-Going Science Team Investigations," *Remote Sensing*, vol. 13, no. 9, p. 1814, May 2021.

[41] J. Thomson, P. Bush, V. Castillo Contreras, N. Clemett, J. Davis, A. De Klerk, E. Iseley, E. J. Rainville, B. Salmi, and J. Talbert, "Development and testing of microSWIFT expendable wave buoys," *Coastal Engineering Journal*, pp. 1–13, 2023.

[42] K. Raghukumar, G. Chang, F. Spada, C. Jones, T. Janssen, and A. Gans, "Performance Characteristics of "Spotter," a Newly Developed Real-Time Wave Measurement Buoy," *Journal of Atmospheric and Oceanic Technology*, vol. 36, no. 6, pp. 1127–1141, Jun. 2019.

[43] C. Dorsay, I. Houghton, J. Davis, J. Thomson, P. Smit, and E. Stackpole, "Aerial Deployment of Spotter Wave Buoys During Hurricane Ian," in *OCEANS 2023 - MTS/IEEE U.S. Gulf Coast*. Biloxi, MS, USA: IEEE, Sep. 2023, pp. 1–5.

[44] P. K. Quinn, E. Thompson, D. J. Coffman, S. Baidar, L. Bariteau, T. S. Bates, S. Bigorre, A. Brewer, G. De Boer, S. P. De Szoeke, K. Drushka, G. R. Foltz, J. Intrieri, S. Iyer, C. W. Fairall, C. J. Gaston, F. Jansen, J. E. Johnson, O. O. Krüger, R. D. Marchbanks, K. P. Moran, D. Noone, S. Pezoa, R. Pincus, A. J. Plueddemann, M. L. Pöhlker, U. Pöschl, E. Quinones Melendez, H. M. Royer, M. Szczodrak, J. Thomson, L. M. Upchurch, C. Zhang, D. Zhang, and P. Zuidema, "Measurements from the RV Ronald H. Brown and related platforms as part of the Atlantic Tradewind Ocean-Atmosphere Mesoscale Interaction Campaign (ATOMIC)," Tech. Rep., 2020.

[45] J. Thomson, "Wave Breaking Dissipation Observed with "SWIFT" Drifters," *Journal of Atmospheric and Oceanic Technology*, vol. 29, no. 12, pp. 1866–1882, Dec. 2012.

[46] E. J. Walsh, C. W. Fairall, and I. PopStefanija, "In the eye of the storm," *Journal of Physical Oceanography*, 2021.

[47] I. PopStefanija, C. W. Fairall, and E. J. Walsh, "Mapping of Directional Ocean Wave Spectra in Hurricanes and Other Environments," *IEEE Transactions on Geoscience and Remote Sensing*, vol. 59, no. 11, pp. 9007–9020, Nov. 2021.

[48] D. Thompson, T. Elfouhaily, and J. Garrison, "An improved geometrical optics model for bistatic GPS scattering from the ocean surface," *IEEE Transactions on Geoscience and Remote Sensing*, vol. 43, no. 12, pp. 2810–2821, Dec. 2005.

[49] R. Pincus, C. W. Fairall, A. Bailey, H. Chen, P. Y. Chuang, G. De Boer, G. Feingold, D. Henze, Q. T. Kalen, J. Kazil, M. Leandro, A. Lundry, K. Moran, D. A. Naeher, D. Noone, A. J. Patel, S. Pezoa, I. PopStefanija, E. J. Thompson, J. Warnecke, and P. Zuidema, "Observations from the NOAA P-3 aircraft during ATOMIC," *Earth System Science Data*, no. 7, pp. 3281–3296, Jul. 2021.

[50] J. Sapp, S. Alsweiss, Z. Jelenak, P. Chang, and J. Carswell, "Stepped Frequency Microwave Radiometer Wind-Speed Retrieval Improvements," *Remote Sensing*, vol. 11, no. 3, p. 214, Jan. 2019.

[51] S. F. Barstow, J.-R. Bidlot, S. Caires, M. A. Donelan, W. M. Drennan, H. Dupuis, H. C. Graber, J. Green, O. Gronlie, and C. Guérin, *Measuring and analysing the directional spectra of ocean waves*. COST Office, 2005.

[52] M. D. Powell, P. J. Vickery, and T. A. Reinhold, "Reduced drag coefficient for high wind speeds in tropical cyclones," *Nature*, vol. 422, no. 6929, pp. 279–283, Mar. 2003.

[53] C. L. Vincent, J. Thomson, H. C. Graber, and C. O. Collins, "Impact of swell on the wind-sea and resulting modulation of stress," *Progress in Oceanography*, vol. 178, Nov. 2019.

[54] D. D. Chen, C. S. Ruf, and S. T. Gleason, "Response time of mean square slope to wind forcing: An empirical investigation," *Journal of Geophysical Research: Oceans*, vol. 121, no. 4, pp. 2809–2823, Apr. 2016.